Journal of the Australian Ceramic Society (2021) 57:1521–1530
https://doi.org/10.1007/s41779-021-00642-w

RESEARCH

Microwave-assisted synthesis of heterostructure Pd/ZnO flowers used for photocatalytic reaction of dyes illuminated by UV radiation

Anukorn Phuruangrat[1] · Areerat Nunpradit[1] · Thawatchai Sakhon[2] · Phattranit Dumrongrojthanath[3] · Nuengruethai Ekthammathat[4] · Somchai Thongtem[5,6] · Titipun Thongtem[5,7]

Received: 2 January 2021 / Revised: 3 August 2021 / Accepted: 4 August 2021 / Published online: 13 September 2021

Abstract

Pd nanoparticles loaded on ZnO flowers were successfully synthesized by microwave-assisted deposition method. Phase, morphology, vibrational mode, composition, oxidation state, and specific surface area of heterostructure Pd/ZnO composites were characterized by X-ray diffraction (XRD), Fourier transform infrared (FTIR) spectroscopy, X-ray photoelectron spectroscopy (XPS), Brunauer–Emmett–Teller (BET) surface area analysis, field emission scanning electron microscopy (FE-SEM), and energy-dispersive X-ray spectroscopy (EDS). Effect of weight content of the loaded Pd on photodegradation of methylene blue (MB) and methyl orange (MO) illuminated by UV radiation was evaluated. Heterostructure Pd/ZnO composites have photocatalytic efficiency higher than hexagonal ZnO flowers. Schottky Pd/ZnO interface played the role in the charge separation process. In this research, heterostructure 5% Pd/ZnO composites have the highest photodegradation of MB and MO under UV radiation. Main active species of the degradation process and stability of the photocatalyst were investigated. A proposed mechanism for photodegradation of MB and MO was also explained.

Keywords Pd/ZnO flowers · Photocatalysis · Main active species · Stability of photocatalyst

Introduction

The rapid development of textile industries and the increase in population lead to the pollution of water reservoirs and destruction of surrounding environment on Earth by the released toxic, indestructible, bio-recalcitrant, mutagenic, carcinogenic, and resistant agents. Thus, the demand of clean water has gradually increased and researchers have investigated effective processes for the removal of toxic agents from wastewater for the survival of lives on Earth [1–3]. Photocatalysis as green technology and environmentally friendly process is broadly useful to purify water by using highly active species and transforming toxic agents into CO_2, H_2O, and mineral salts under solar radiation [1, 4, 5].

Zinc oxide (ZnO) as an n-type semiconductor with 3.37-eV broad bandgap has been considered as a promising photocatalyst used for decontaminating liquid waste. It is nontoxic, inexpensive, chemically and physically stable, easy to prepare, and very active. ZnO has been widely studied for enhanced photocatalytic performance under ultraviolet (UV) radiation [1, 2, 4, 6]. Nevertheless, its disadvantage is fast recombination of electron–hole pairs that produce

✉ Anukorn Phuruangrat
phuruangrat@gmail.com

✉ Somchai Thongtem
schthongtem@yahoo.com

1 Division of Physical Science, Faculty of Science, Prince of Songkla University, Hat Yai, Songkhla 90112, Thailand

2 Electron Microscopy Research and Service Center, Faculty of Science, Chiang Mai University, Chiang Mai 50200, Thailand

3 Rajamangala University of Technology Lanna Chiang Rai, Chiang Rai 57120, Thailand

4 Program in Chemistry, Faculty of Science and Technology, Bansomdejchaopraya Rajabhat University, Bangkok 10600, Thailand

5 Materials Science Research Center, Faculty of Science, Chiang Mai University, Chiang Mai 50200, Thailand

6 Department of Physics and Materials Science, Faculty of Science, Chiang Mai University, Chiang Mai 50200, Thailand

7 Department of Chemistry, Faculty of Science, Chiang Mai University, Chiang Mai 50200, Thailand

active radicals for photodegradation of toxic reagents [1, 7, 8]. Thus, loading of noble metal nanoparticles such as Au, Pd, and Ag on ZnO semiconductor has been studied to delay the recombination of photo-generated charge carriers and to enhance photocatalytic efficiency [5, 9–12]. For example, Fageria et al. succeeded in loading of Au and Ag nanoparticles on the surface of ZnO nanoflowers using hydrazine hydrate as a reducing agent [10]. They found that photodegradation of methylene blue (MB) was improved by the loaded nanoparticles illuminated by UV and visible light because the nanoparticles effectively accepted electrons from conduction band (CB) and the immediate recombination process was prevented in accordance with other reports [11–13]. Zhang et al. successfully prepared Pd/ZnO composites by a facile one-pot solvothermal method [13]. They found that Pd/ZnO composites show good photocatalytic performance and have high stability in degrading organic pollutant due to the effective separation of electron–hole pairs and the highly active surface area.

In this research, a facile and simple microwave-assisted deposition method was used to synthesize 0–10% Pd/ZnO samples. Effect of the loaded Pd on hierarchical ZnO microspherical flowers on photocatalytic reaction was studied through the degradation of methylene blue (MB) and methyl orange (MO) under UV light illumination. Phase and morphology of heterostructure Pd/ZnO composites were characterized by X-ray diffraction (XRD), Fourier transform infrared (FTIR) spectroscopy, X-ray photoelectron spectroscopy (XPS), Brunauer–Emmett–Teller (BET) surface area analysis, field emission scanning electron microscopy (FE-SEM), and energy-dispersive X-ray spectroscopy (EDS). The analytical results show that metallic Pd^0 spherical nanoparticles were supported on hierarchical ZnO spherical microflowers. Heterostructure 5% Pd/ZnO composites played the role in degrading dye higher than other samples. Stability of the photocatalyst and active radicals used for photodegradation of MB and MO over the as-prepared heterostructure Pd/ZnO composites were investigated. A mechanism for the photodegradation of MB and MO dyes was also explained.

Experiment

Flower-like ZnO samples were prepared by direct precipitation method. In 200 ml reverse osmosis (RO) water, 13.3866 g $Zn(NO_3)_2{\cdot}6H_2O$ was dissolved with continued stirring at room temperature. Subsequently, 40 ml of 3 M NaOH solution was added to the Zn^{2+} solution with vigorous stirring for 24 h to form white precipitates. The as-prepared precipitates were filtered, washed, dried, and heated at 600 °C by 5 °C min^{-1} heating rate in ambient atmosphere for 2 h.

To prepare Pd/ZnO composites, $PdCl_2$ with 1%, 5%, and 10% by weight of Pd was dissolved in 100 ml ethylene glycol containing 2.5 g ZnO suspension with constant stirring for 30 min. The mixtures were heated in 150-W microwave for 30 min. The as-prepared samples were collected, washed with deionized water, and dried for further characterization.

Crystalline phase of the as-synthesized samples was characterized by an X-ray diffractometer (XRD, Philips X'Pert MPD) using Cu-K_α radiation in the range of 20–60°. Morphological investigation was carried out by a field emission scanning electron microscope (FE-SEM, JEOL JSM-6335F) at an acceleration voltage of 20 kV coupled with an Oxford INCA energy-dispersive X-ray spectrometer (EDS). A Fourier transform infrared (FTIR) spectrometer (Bruker Tensor 27) was carried out in the range of 400–4000 cm^{-1} at room temperature. ZnO pellets were prepared by 40 times KBr dilution for FTIR testing. X-ray photoelectron spectroscopy (XPS) was carried out by a Kratos X-ray photoelectron spectrometer—Axis Ultra DLD—with a monochromated Al K_α radiation (1486.6 eV) as a providing source. All the XPS spectra were calibrated w.r.t. a C 1 s electron peak at 285.1 eV. Surface areas of the samples were analyzed by nitrogen adsorption–desorption isotherm at 80 °C by a Quantachrome Autosorb 1 MP automatic gaseous adsorption system and calculated through the basis of Brunauer–Emmett–Teller (BET) surface area analysis.

Cationic methylene blue (MB) and anionic methyl orange (MO) were used as molecular probes for photocatalytic evaluation. The photocatalytic reaction was conducted at room temperature under UV light. The reaction was carried out using 200-mg catalyst dispersed in 200 ml of 1×10^{-5} M dye aqueous solution. Prior to irradiation, the suspension solutions were magnetically stirred in the dark for 30 min to establish an adsorption/desorption equilibrium of dye and photocatalyst. During photocatalytic testing, approximately 5-ml solutions were withdrawn every 20 min and centrifuged to remove any suspended catalytic nanoparticles. The residual contents of MB/MO dyes containing in the cuvettes were measured at 664 nm for MB degradation and 464 nm for MO degradation with de-ionized water as a reference by a UV–visible spectrophotometer (Perkin-Elmer Lambda 25). The decolorization efficiency was calculated by the below equation.

$$Decolorization\ efficiency(\%) = \frac{C_o - C_t}{C_o} \times 100 \quad (1)$$

C_o is the initial dye concentration and C_t is the dye concentration after photocatalytic treatment for a period of time (t). Stability of the photocatalyst was tested for five cycles. At the end of each photocatalytic cycle, the re-used heterostructure Pd/ZnO composites were centrifuged, washed, and dried for the next test for MB and MO degradation.

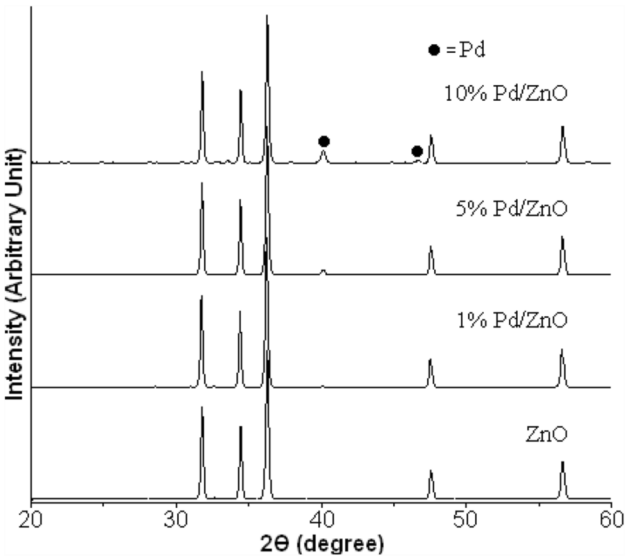

Fig. 1 XRD patterns of ZnO flowers containing different weight contents of Pd nanoparticles

Results and discussion

Phase and composition of ZnO containing different weight contents of Pd were examined by XRD as the results shown in Fig. 1. The XRD pattern of pure ZnO without the loaded Pd shows five diffraction peaks at 2θ of 31.83°, 34.46°, 36.30°, 47.54°, and 56.68° which can be indexed to the (100), (002), (101), (102), and (110) planes of wurtzite hexagonal ZnO structure with $P6_3mc$ space group (JCPDS no. 36–1451 [14]), respectively. The diffraction pattern of pure ZnO sample was composed of sharp peaks with no detection of impurity phase. Thus, the pure ZnO sample is single phase with high crystalline degree. When 1%, 5%, and 10% by weight of Pd were loaded on top of ZnO, additional diffraction peaks at 2θ of 40.16° and 46.67° for heterostructure 5% and 10% Pd/ZnO composites were detected and can be indexed to the (111) and (200) planes of face-centered cubic (FCC) Pd structure with Fm-3 m space group (JCPDS no. 46–1043 [14]). No Pd peaks of the 1% Pd/ZnO composites were detected because the Pd content is too low to be detected by the XRD. Comparing the diffraction peaks of Pd and ZnO of heterostructure 10% Pd/ZnO composites, the main diffraction peak of ZnO is higher than that of Pd. The results indicate that hexagonal ZnO is the majority and FCC Pd is the minority. The crystallite sizes of ZnO and Pd on heterostructure Pd/ZnO composites were calculated by the below Scherrer equation.

$$D = K\lambda/\beta cos\theta \quad (2)$$

D is the crystallite size of the crystal, K is a dimensionless constant ($K = 0.89$ for spherical particle), λ is the wavelength of Cu K_α (0.154056 nm), β is the full width at half-maximum (FWHM) of the main diffraction peak of the crystal, and θ is the diffraction angle of the main diffraction peak [3, 13, 15, 16]. The calculated crystallite sizes of ZnO, 1% Pd/ZnO, 5% Pd/ZnO, and 10% Pd/ZnO were 95.78, 95.78, 95.78, and 79.82 nm, while those of Pd on Pd/ZnO composites were 25.57 and 26.78 nm for 5% and 10% Pd/ZnO composites, respectively.

Figure 2 shows FTIR spectra of pure ZnO sample and heterostructure Pd/ZnO composites diluted with KBr in the wavenumber range of 400–4000 cm^{-1}. They show the broad absorption bands at 3400–3600 cm^{-1} in all samples which are assigned to the OH stretching of adsorbed water on the top [1, 3, 5, 6, 17]. The sharp FTIR bands of pure ZnO sample and heterostructure Pd/ZnO composites at 429, 426, 425, and 425 cm^{-1} for 0%, 1%, 5%, and 10% Pd/ZnO samples were assigned to the characteristic Zn–O bond of ZnO lattice [1, 3, 4]. The vibration of Zn–O bond of heterostructure Pd/ZnO composites was little shifted to lower wavenumber due to the interaction between Pd and ZnO.

Surface compositions and chemical states of the as-prepared pure ZnO sample and heterostructure 5% and 10% Pd/ZnO composites were investigated by XPS using C 1 s at 285.1 eV as a reference as the results shown in Fig. 3. The full-scan XPS spectra of as-prepared pure ZnO sample and heterostructure 5% and 10% Pd/ZnO composites show the binding energy signals of Zn and O of ZnO and additional signal of Pd on heterostructure 5% and 10% Pd/ZnO composites. Zn and O elements were detected in pure ZnO sample with additional Pd in the heterostructure 5% and 10% Pd/ZnO composites. C 1 s as a reference was also detected in all samples. Thus, the samples are very pure.

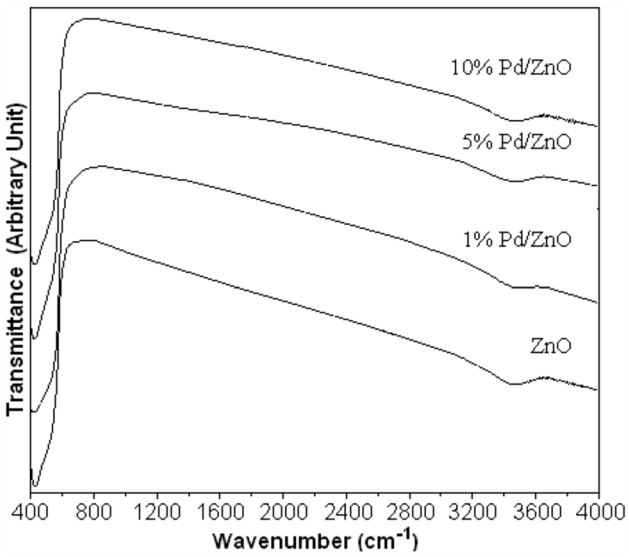

Fig. 2 FTIR spectra of ZnO flowers containing different weight contents of Pd nanoparticles

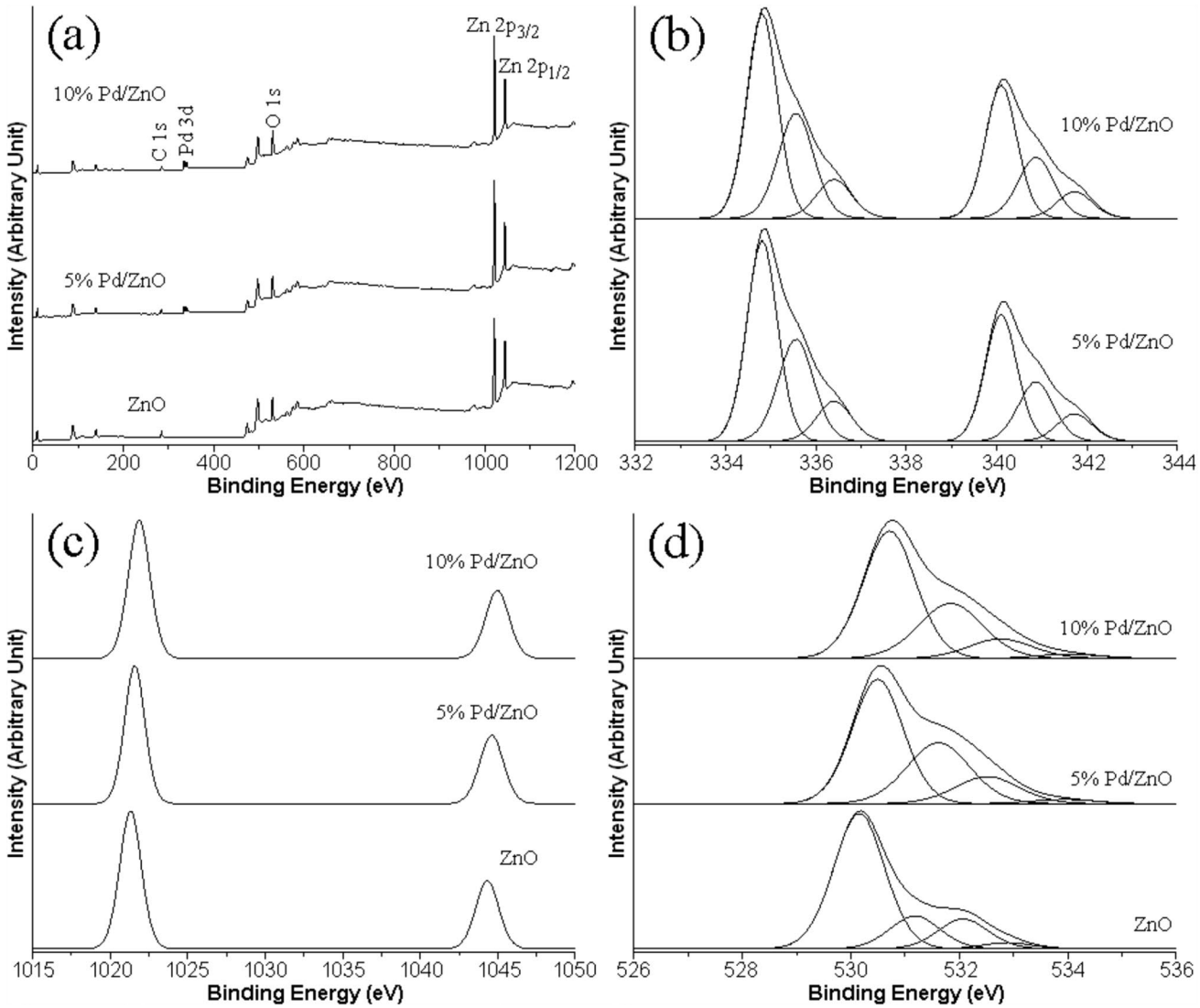

Fig. 3 **a** XPS survey spectra and **b–d** high-resolution XPS spectra of Pd 3d, Zn 2p, and O 1 s of ZnO, 5% Pd/ZnO, and 10% Pd/ZnO flowers, respectively

The high-resolution XPS spectra of Pd 3d core levels of heterostructure 5% and 10% Pd/ZnO composites show binding energy peaks of Pd $3d_{5/2}$ at 334.60 eV and Pd $3d_{3/2}$ at 339.94 eV corresponding to the characteristic metallic Pd^0. The results indicate that metallic Pd^0 was successfully loaded on ZnO samples by reduction of Pd^{2+} containing in ethylene glycol [13, 18–21]. Comparing with the bulk metallic Pd (335.1 eV for Pd $3d_{5/2}$ and 340.4 eV for Pd $3d_{3/2}$) [20, 21], the Pd 3d binding energies of heterostructure 5% and 10% Pd/ZnO composites were shifted to the lower binding energy side due to the interaction between Pd and ZnO of heterostructure 5% and 10% Pd/ZnO composites. Thus, charge diffusion from ZnO to Pd was proceeding at the Pd/ZnO Schottky interface and the photocatalytic performance was enhanced [20, 21]. They should be noted that the minor binding energies of Pd $3d_{5/2}$ and Pd $3d_{3/2}$ core levels of heterostructure 5% and 10% Pd/ZnO composites were detected at 335.36 eV and 340.82 eV for Pd^{2+} and 336.23 eV and 341.75 eV for Pd^{4+} possibly caused by the oxidation of Pd^0 on top of ZnO during the XPS analysis [18, 19, 21]. Some Pd with + 2 and + 4 oxidation states may contain in the heterostructure Pd/ZnO composites [2, 3, 13, 22] although they are not analyzed by XPS. The high-resolution spectra of Zn 2p core levels consisted of two binding energy peaks centered at 1021.32 eV and 1044.32 eV for Zn $2p_{3/2}$ and Zn $2p_{1/2}$ for pure ZnO sample and 1021.58 eV and 1044.58 eV for Zn $2p_{3/2}$ and Zn $2p_{1/2}$ for heterostructure 5% and 10% Pd/ZnO composites [2, 3, 13, 22]. The binding energy separation of Zn $2p_{3/2}$ and Zn $2p_{1/2}$ is 23 eV in accordance with previous reports [2, 3, 13, 22]. The asymmetrical high-resolution

spectra of O 1 s core level of the samples were analyzed by a Gaussian deconvolution method. They contain four peaks at 530.16 eV, 531.18 eV, 532.08 eV, and 532.89 eV for pure ZnO sample and 530.49 eV, 531.63 eV, 532.51 eV, and 533.91 eV for heterostructure 5% and 10% Pd/ZnO composites. They were ascribed to the Zn–O bond of ZnO lattice and O–O, O–H and C–O of chemically adsorbed oxygen and adsorbed H_2O and CO_2 on the top [2, 3, 13, 22].

Morphologies of the as-prepared pure ZnO sample and heterostructure 1%, 5%, and 10% Pd/ZnO composites were investigated by SEM as the results shown in Fig. 4. The SEM image of pure ZnO sample shows uniform hierarchical spherical microflowers with 1–3-μm diameter. An individual hierarchical spherical microflower is the assembly of nanoplate petals which are 100–150-nm thick. Clearly, nanoplates were closely packed layer by layer from centers of clusters and were built up to spherical microflowers. Moreover, there are a large amount of holes between petals, which greatly enlarge the surface area for organic dye adsorption on ZnO microflowers. When Pd nanoparticles were loaded on ZnO microflowers, the heterostructure 1% and 5% Pd/ZnO composites were still remaining as hierarchical spherical microflowers of self-assembled nanopetals with rough surfaces. Pd nanoparticles with particle size of less than 50 nm were supported on the surface of hierarchical spherical ZnO microflowers. The separation of photo-induced charge carriers was effectively improved and the photocatalytic activity was also promoted. They should be noted that the surface petals were roughened when Pd nanoparticles were loaded on the top. The attached Pd nanoparticles connected voids between petals of ZnO spherical microflowers. Thus, the surface of ZnO spherical microflowers was reduced. According to the BET analysis, the surface area of ZnO was continuously decreased in sequence as follows: 37.42 $m^2.g^{-1}$, 33.07 $m^2.g^{-1}$, 30.83 $m^2.g^{-1}$, and 25.32 $m^2.g^{-1}$ for 0%, 1%, 5%, and 10% Pd/ZnO, respectively. The surface area of sample was decreased with the increase of the loaded Pd nanoparticles because the deposited Pd nanoparticles played the role in reducing voids of hierarchical spherical ZnO microflowers as the above explanation. The Pd nanoparticles were fully loaded on the 10% hierarchical Pd/ZnO microflowers. The elemental EDS map of heterostructure 5% Pd/ZnO composites is shown in Fig. 5. In this research, Pd, Zn, and O elements of heterostructure 5% Pd/ZnO composites were detected and the Pd nanoparticles were uniformly distributed across the ZnO nanopetals.

Photocatalysis of pure ZnO and heterostructure Pd/ZnO samples were evaluated through the degradation of MB and MO under UV light irradiation. Figures 6 and 7 show the change of UV–visible absorption of MB and MO over pure ZnO and heterostructure 1%, 5%, and 10% Pd/ZnO samples within different lengths of UV irradiation time. Clearly, the intensities of MB and MO absorbance over heterostructure 5% Pd/ZnO composites were the lowest within 100 min and the degradation rates of MB and MO over heterostructure 5% Pd/ZnO composites were the highest. The characteristic peaks of MB at 664 nm and MO at 464 nm were gradually decreased with increasing in the irradiation time. In

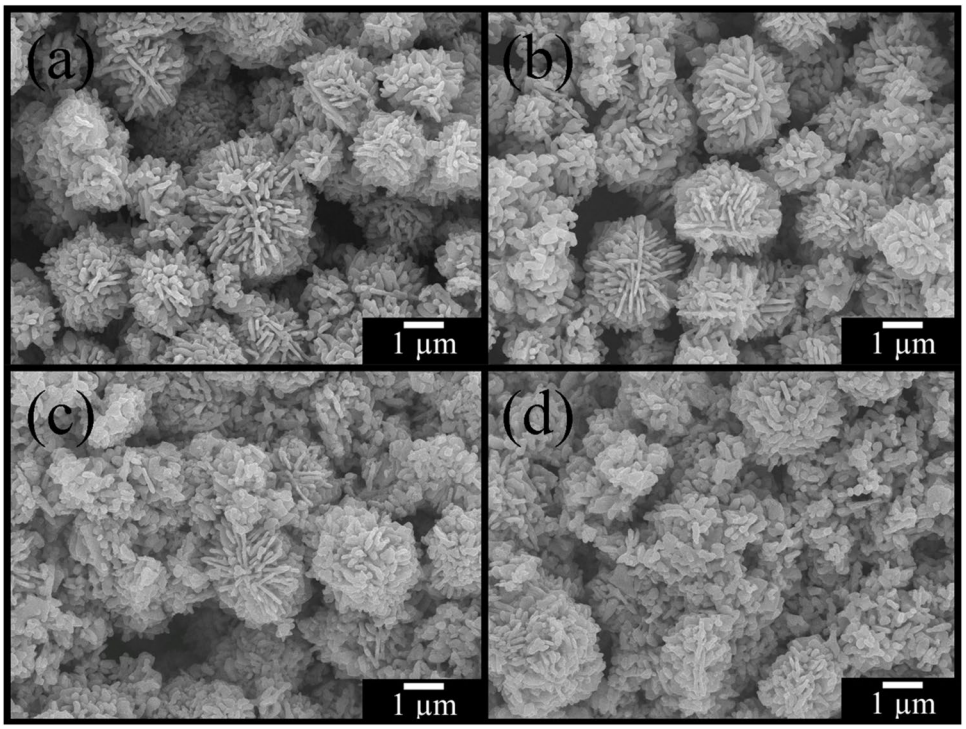

Fig. 4 SEM images of **a** pure ZnO, **b** 1% Pd/ZnO, **c** 5% Pd/ZnO, and **d** 10% Pd/ZnO samples

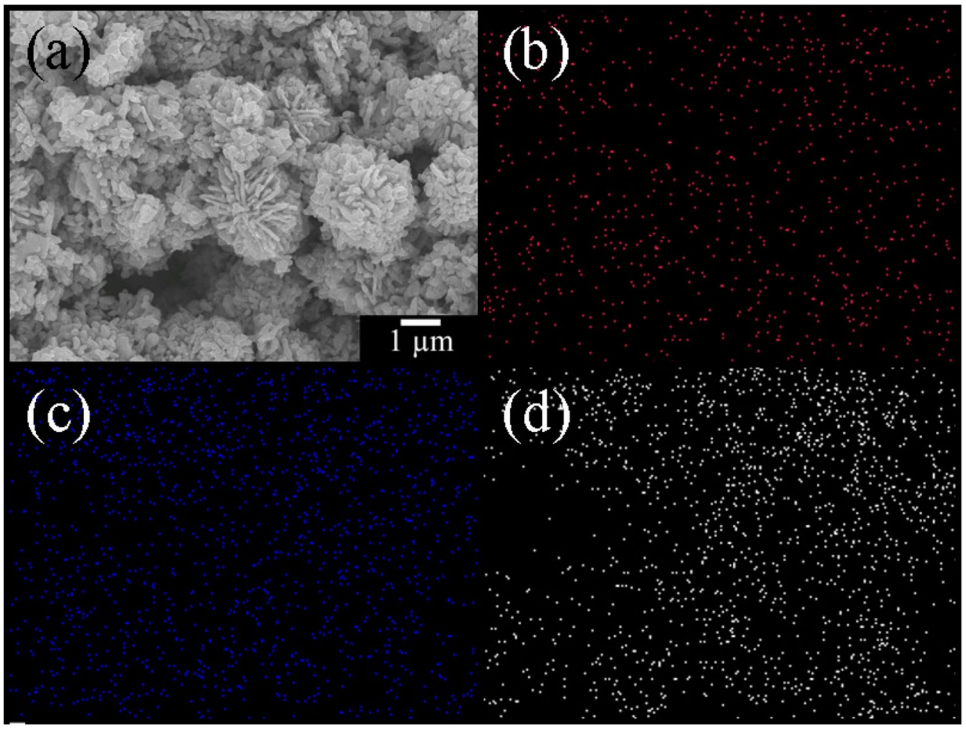

Fig. 5 **a** SEM image and EDS map of **b** Pd, **c** Zn, and **d** O of 5% Pd/ZnO flowers

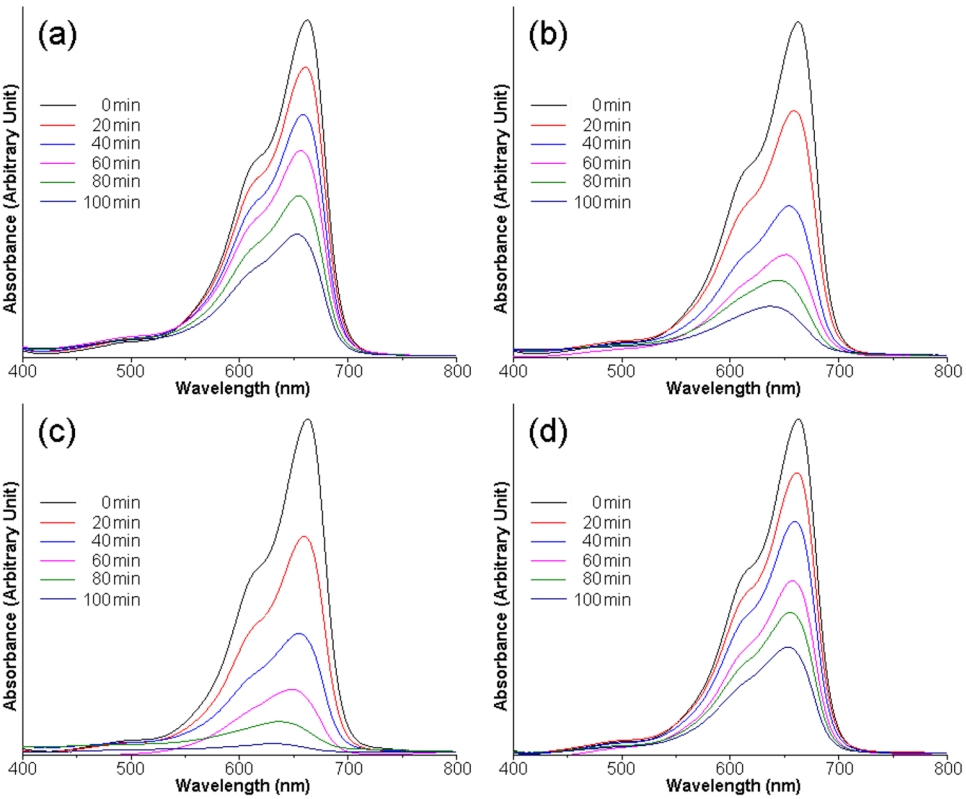

Fig. 6 UV–visible absorption of MB photocatalyzed by **a** 0%, **b** 1%, **c** 5%, and **d** 10% Pd/ZnO flowers under UV light irradiation

this research, MB and MO were completely degraded over heterostructure 5% Pd/ZnO composites within 100 min irradiation time.

Figure 8a and b shows the photocatalytic effectiveness of as-prepared ZnO containing different weight contents of Pd in degrading of MB and MO illuminated by UV radiation.

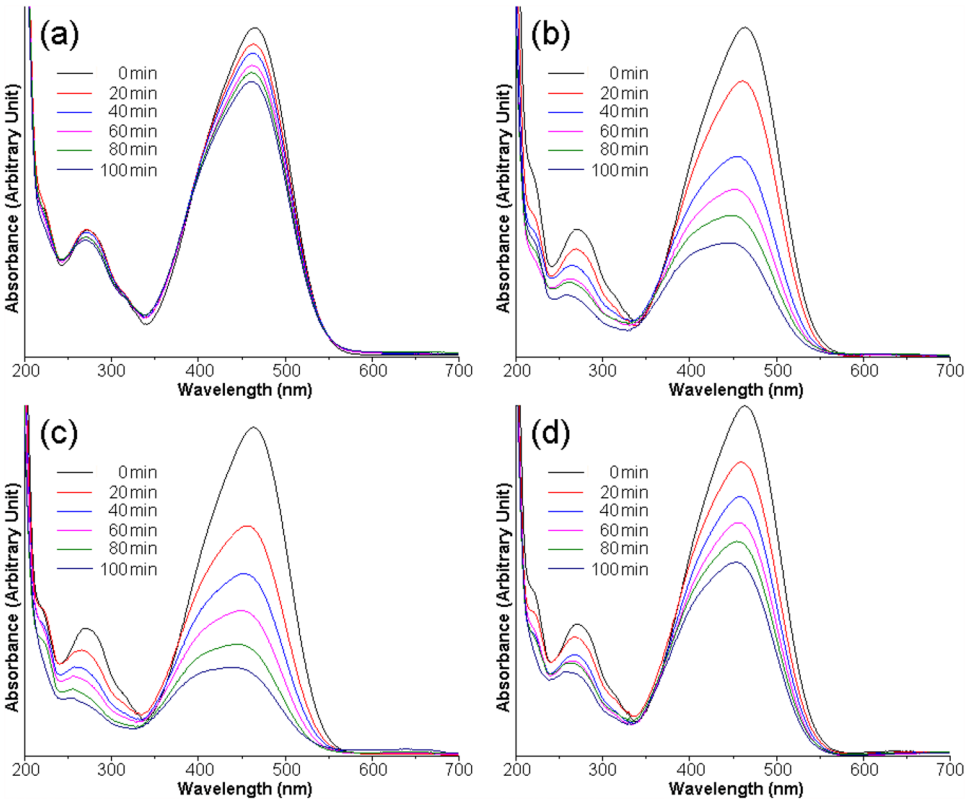

Fig. 7 UV–visible absorption of MO photocatalyzed by **a** 0%, **b** 1%, **c** 5%, and **d** 10% Pd/ZnO flowers under UV light irradiation

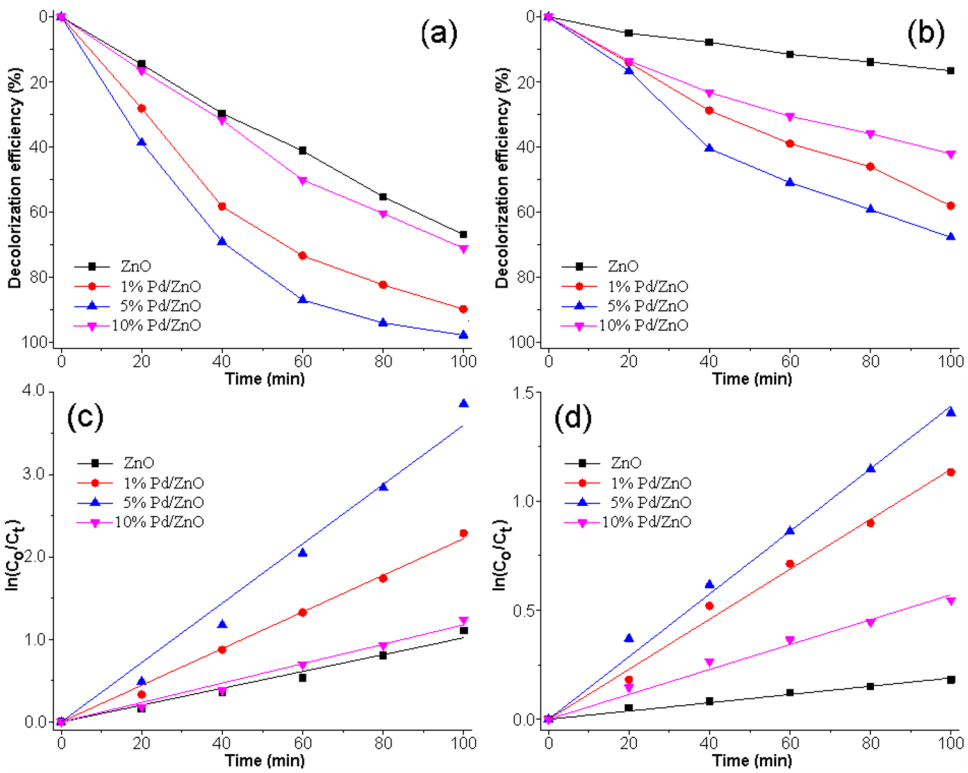

Fig. 8 Decolorization efficiencies and pseudo-first-order plots for photodegradation of **a**, **c** MB and **b**, **d** MO over ZnO flowers containing different weight contents of Pd nanoparticles

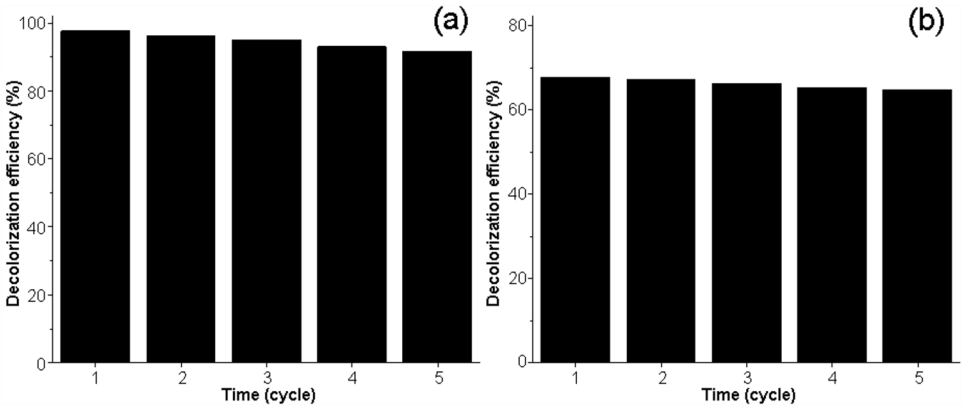

Fig. 9 Photodegradation of **a** MB and **b** MO over the re-used 5% Pd/ZnO flowers illuminated by UV radiation for five cycles

Pure ZnO sample has the photodegradation of both MB and MO less than the heterostructure Pd/ZnO composites. Obviously, the photocatalytic activity of heterostructure Pd/ZnO composites gradually increases to the highest at 5% Pd and decreases after being loaded with 10% Pd nanoparticles. The heterostructure 5% Pd/ZnO composites have the highest photodegradation of 97.88% MB and of 67.79% MO under UV light irradiation within 100 min because Pd nanoparticles as electron sinks played the role in reducing the recombination of photo-generated electron–hole pairs and enhancing the photocatalytic efficacy of ZnO sample [10, 18, 19, 23]. The photocatalytic performance of heterostructure 10% Pd/ZnO composites was reduced because the excessive Pd nanoparticles blocked the UV light on top of hierarchical ZnO spherical microflowers [24]. Figure 8c and d shows the linear plot of $\ln(C_o/C_t)$ versus reaction time over pure ZnO and heterostructure Pd/ZnO samples. The data points were fitted to linear lines according to the pseudo-first-order kinetics [4, 7, 22, 23]. The pseudo-first-order rate constant (k) for photodegradation of MB and MO over a photocatalyst was calculated from the slope of linear line [4, 7, 22]. In this research, heterostructure 5% Pd/ZnO composites have the highest rate constant of 0.0362 min^{-1} for MB and 0.0142 min^{-1} for MO. The rate constants for MB and MO are 3.55 and 7.32 times of pure ZnO sample ($k = 0.0102$ min^{-1} for MB and 1.94×10^{-3} min^{-1} for MO) because the separation of photo-generated electron–hole pairs was increased by the loaded Pd nanoparticles.

The photocatalytic stability of reused heterostructure 5% Pd/ZnO composites was studied for five cycles as the results shown in Fig. 9. The photocatalytic efficiencies of reused heterostructure 5% Pd/ZnO composites were 97.88%, 96.38%, 95.35%, 93.25%, and 91.85% for the 1st, 2nd, 3rd, 4th, and 5th cycle for MB degradation and 67.79%, 67.21%, 66.25%, 65.31%, and 64.78% for the 1st, 2nd, 3rd, 4th, and 5th recycle for MO degradation under UV light irradiation. The efficiencies at the end of cycle five were 0.94 and 0.96 times those at the end of cycle one for MB and MO degradation, respectively. The results certify that heterostructure 5% Pd/ZnO composites are stable under UV light irradiation. XRD patterns of the reused heterostructure 5% Pd/ZnO composites at the end of cycle five are shown in Fig. 10. The analysis shows that the photocatalyst used for MB and MO degradation for five cycles remained as the Pd/ZnO composites. The lattice parameters of ZnO and Pd of 5% Pd/ZnO composites before photocatalytic test and after ending of cycle five were concluded in Table 1 and were almost

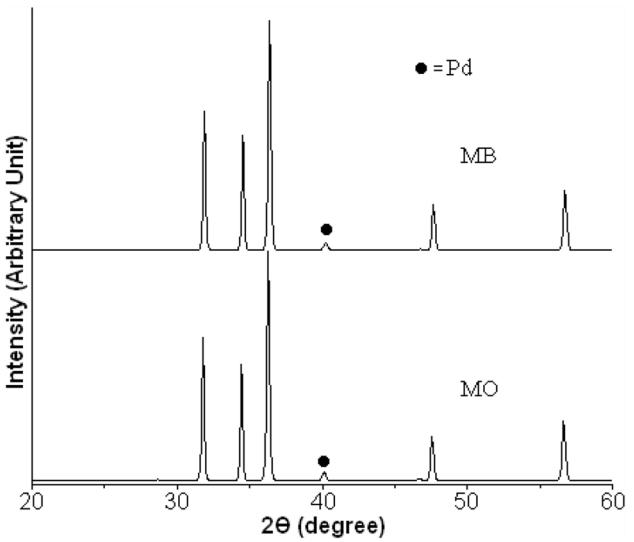

Fig. 10 XRD patterns of 5% Pd/ZnO flowers after being used for photocatalytic test of MB and MO degradation for five cycles

Table 1 Lattice parameters of ZnO flowers and Pd nanoparticles containing 5% Pd/ZnO composites before and after being used for photocatalytic reaction

Photocatalytic reaction	Hexagonal ZnO flowers		FCC Pd nanoparticles
	a (Å)	c (Å)	a (Å)
Before	3.2444 ± 0.0011	5.2012 ± 0.0009	3.8875 ± 0.0023
After	3.2448 ± 0.0015	5.2014 ± 0.0008	3.8853 ± 0.0018

unchanged. Thus, heterostructure 5% Pd/ZnO composites are very stable even at the end of cycle five and are excellent in practical application for photodegradation of the MB and MO dyes.

To understand the mechanism for photodegradation of dyes over 5% Pd/ZnO under UV light irradiation, active species as h^+, OH, and O_2^- of the photocatalytic process were determined by adding TEOA (h^+ scavenger), IPA (OH scavenger) and BQ (O_2^- scavenger) to the photocatalytic solutions [2, 4, 25, 26]. Figure 11 shows the photodegradation of MB and MO solutions with and without scavengers over Pd/ZnO composites under UV light irradiation. They can be seen that the decolorization efficiencies for the dye solutions containing IPA and BQ under UV light irradiation were significantly decreased to 32.78% and 18.95% for MB degradation and 28.57% and 13.78% for MO degradation. When TEOA was added in the MB and MO solutions, the decolorization efficiencies were not much changed. In conclusion, OH, and O_2^- radicals are the main active species used for photodegradation of MB and MO dyes over 5% Pd/ZnO composites under UV light irradiation.

When ZnO flowers absorbed photon with $E \geq E_{g(ZnO)}$, electrons in valence band (VB) were excited to conduction band (CB) and holes were induced in VB [10, 11, 27]. Photo-excited electrons of CB migrated through the Pd/ZnO interface to Pd nanoparticles (electron sinks). Photo-induced holes of VB migrated to the surface of ZnO flowers. The electrons reacted with adsorbed oxygen (O_2) and the holes reacted with hydroxide anions (OH^-) and/or water (H_2O) to form superoxide anion (O_2^-) and hydroxyl (OH) radicals as strong oxidants used for photodegradation of MB/MO dyes in wastewater [10, 11, 27]. These active radicals played the role in degrading of MB/MO molecules by transforming MB/MO into CO_2, H_2O, and small inorganic ions. The photocatalytic performance of ZnO is quite low because of the high recombination rate and the short lifetime of electron–hole pairs [10, 18, 19, 28]. The recombination rate of electrons–holes of the composites was reduced and the separation of electrons–holes was promoted. The production rate of O_2^- and OH radicals and the photocatalytic efficiency of heterostructure Pd/ZnO composites were enhanced [10, 18, 19, 28]. The reaction for photodegradation of MB/MO dyes over heterostructure Pd/ZnO composites can be written as follows [10, 18, 19, 28].

$$ZnO + hv\left(E \geq E_g\right) \rightarrow e^-{}_{CB} + h^+{}_{VB} \tag{3}$$

$$Pd + e^-{}_{CB} \rightarrow e^-{}_{Pd} \tag{4}$$

$$e^-{}_{Pd} + O_2 \rightarrow {}^{\bullet}O_{2^-} \tag{5}$$

$$h^+{}_{VB} + OH^-/H_2O \rightarrow {}^{\bullet}OH/\left({}^{\bullet}OH + H^+\right) \tag{6}$$

$$2H^+ + 2e^-{}_{CB} \rightarrow H_2(g) \tag{7}$$

$$H^+ + HO^- \rightarrow H_2O \tag{8}$$

$${}^{\bullet}O_2^-/{}^{\bullet}OH + MB/MO \rightarrow CO_2 + H_2O + small\ inorganic\ ions \tag{9}$$

The results indicate that heterostructure Pd/ZnO composites have photocatalytic activity higher than pure ZnO sample because metallic Pd nanoparticles act as electron acceptor and therefore promote the effective separation of electron–hole pairs.

Conclusions

In summary, the heterostructure Pd/ZnO composites were successfully synthesized by the microwave-assisted deposition method. According to the analytical results, FCC metallic Pd nanoparticles were loaded on the surface of hierarchical ZnO spherical microflowers. The heterostructure 5% Pd/ZnO composites have the highest photocatalytic efficiency for the MB/MO degradation under UV light irradiation because metallic Pd nanoparticles acted as electron sinks

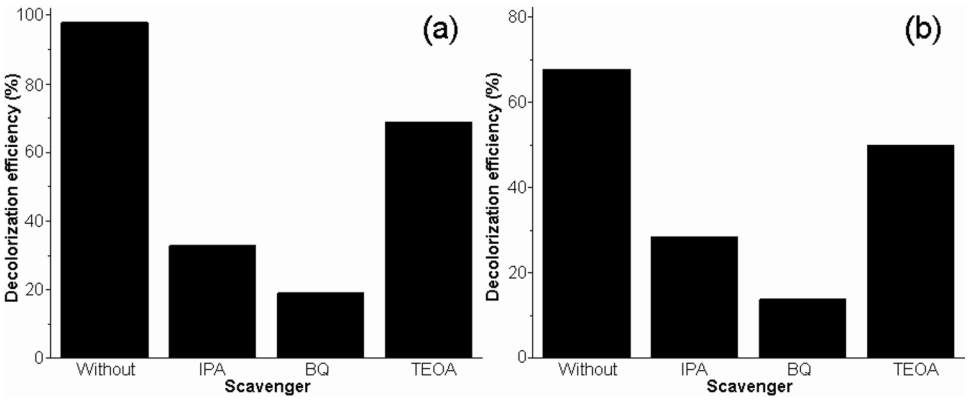

Fig. 11 Photodegradation of **a** MB and **b** MO solutions with and without different scavengers photocatalyzed by heterostructure 5% Pd/ZnO flowers illuminated by UV radiation

by promoting charge migration through Pd/ZnO interface. The Pd/ZnO composites are very stable although they were dispersed in the MB/MO solutions under UV light irradiation and are excellent for photodegradation of the dyes.

Funding The research was supported by the Prince of Songkla University, and the Program Management Unit for Human Resources & Institutional Development, Research and Innovation, Office of National Higher Education Science Research, and Innovation Policy Council (NXPO) [Grant Number B16F640001].

References

1. Zarezadeh, S., Habibi-Yangjeh, A., Mousavi, M., Ghosh, S.: Novel ZnO/Ag_3PO_4/AgI photocatalysts: Preparation, characterization, and the excellent visible-light photocatalytic performances. Mater. Sci. Semicond. Process. **119**, 105229 (2020)
2. Koutavarapu, R., Babu, B., Reddy, C.V., Reddy, I.N., Reddy, K.R., Rao, M.C., Aminabhavi, T.M., Cho, M., Kim, D., Shim, J.: ZnO nanosheets-decorated Bi_2WO_6 nanolayers as efficient photocatalysts for the removal of toxic environmental pollutants and photoelectrochemical solar water oxidation. J. Environ. Manage. **265**, 110504 (2020)
3. Kaliraj, L., Ahn, J.C., Rupa, E.J., Abid, S., Lu, J., Yang, D.C.: Synthesis of panos extract mediated ZnO nano-flowers as photocatalyst for industrial dye degradation by UV illumination. J. Photochem. Photobiol. B. **199**, 111588 (2019)
4. Moraes, N.P., Santos, G.S., Neves, G.C., Valim, R.B., Rocha, R.S., Landers, R., Silva, M.L.C.P., Rodrigues, L.A.: Development of Nb_2O_5-doped ZnO/Carbon xerogel photocatalyst for the photodegradation of 4-chlorophenol. Optik. **219**, 165238 (2020)
5. Elhalil, A., Elmoubarki, R., Farnane, M., Machrouhi, A., Mahjoubi, F.Z., Sadiq, M., Qourzal, S., Abdennouri, M., Barka, N.: Novel Ag-ZnO-$La_2O_2CO_3$ photocatalysts derived from the layered double hydroxide structure with excellent photocatalytic performance for the degradation of pharmaceutical compounds. J. Sci. Ad. Mater. Dev. **4**, 34–46 (2019)
6. Meroni, D., Gasparini, C., Michele, A.D., Ardizzone, S., Bianchi, C.L.: Ultrasound-assisted synthesis of ZnO photocatalysts for gas phase pollutant remediation: Role of the synthetic parameters and of promotion with WO_3. Ultrason. Sonochem. **66**, 105119 (2020)
7. Onkani, S.P., Diagboya, P.N., Mtunzi, F.M., Klink, M.J., Olu-Owolabi, B.I., Pakade, V.: Comparative study of the photocatalytic degradation of 2–chlorophenol under UV irradiation using pristine and Ag-doped species of TiO_2, ZnO and ZnS photocatalysts. J. Environ. Manage. **260**, 110145 (2020)
8. Mohammed, M.K.A.: Carbon nanotubes loaded ZnO/Ag ternary nanohybrid with improved visible light photocatalytic activity and stability. Optik. **217**, 164867 (2020)
9. Fernando, J.F.S., Shortell, M.P., Firestein, K.L., Zhang, C., Larionov, K.V., Popov, Z.I., Sorokin, P.B., Bourgeois, L., Waclawik, E.R., Golberg, D.V.: Photocatalysis with Pt−Au−ZnO and Au−ZnO hybrids: effect of charge accumulation and discharge properties of metal nanoparticles. Langmuir. **34**, 7334–7345 (2018)
10. Fageria, P., Gangopadhyay, S., Pande, S.: Synthesis of ZnO/Au and ZnO/Ag nanoparticles and their photocatalytic application using UV and visible light. RSC Adv. **4**, 24962 (2014)
11. Rehman, N., Mehmood, M., Ali, S.M., Ramay, S.M., Alkhuraiji, T.S.: Au/ZnO hybrid composites and their optical and photocatalytic properties. Appl. Phys. A. **126**, 710 (2020)
12. Hosseini-Sarvari, M., Bazyar, Z.: Selective visible-light photocatalytic aerobic oxidation of alkenes to epoxides with Pd/ZnO nanoparticles. ChemistrySelect. **5**, 8853–8857 (2020)
13. Zhang, Y., Wang, Q., Xu, J., Ma, S.: Synthesis of Pd/ZnO composites with high photocatalytic performance by a solvothermal method. Appl. Surf. Sci. **258**, 10104–10109 (2012)
14. Powder Diffract. File, JCPDS Internat. Centre Diffract. Data, PA 19073–3273, U.S.A. (2001).
15. Rubel, M.H.K., Hossain, M.E., Parvez, M.S., Rahaman, M.M., Islam, M.S., Kumada, N., Kojima, S.: Low-temperature synthesis of potassium triniobate (KNb_3O_8) ceramic powder by a novel aqueous organic gel route. J. Aust. Ceram. Soc. **55**, 759–764 (2019)
16. Pandey, S., Kumar, A., Singh, N.B., Mandal, K.D.: Studies on dielectric and magnetic properties of $CaCu_3Ti_3MnO_{12}$ ceramic synthesized via semi-wet route. J. Aust. Ceram. Soc. **56**, 915–922 (2020)
17. Öksüz, K.E., Kilinç, S., Özer, A.: Effect of calcination on microstructure development and properties of hydroxyapatite powders extracted from human and bovine bones. Trans. Indian Ceram. Soc. **78**, 41–45 (2019)
18. Phuruangrat, A., Klangnoi, T., Patiphatpanya, P., Dumrongrojthanath, P., Thongtem, S., Thongtem, T.: Sonochemical-assisted deposition synthesis of visible-light-driven Pd/Bi_2MoO_6 used for photocatalytic degradation of rhodamine B. J. Electron. Mater. **49**, 3684–3691 (2020)
19. Phuruangrat, A., Klangnoi, T., Patiphatpanya, P., Dumrongrojthanath, P., Thongtem, S., Thongtem, T.: Synthesis of Pd nanoparticles modified Bi_2MoO_6 nanoplates by microwave-assisted deposition with their enhanced visible-light-driven photocatalyst. Optik **212**, 164674 (2020)
20. Imran, M., Yousaf, A.B., Zhou, X., Jiang, Y.F., Yuan, C.Z., Zeb, A., Jiang, N., Xu, A.W.: Pd/TiO nanocatalyst with strong metal−support interaction for highly efficient durable heterogeneous hydrogenation. J. Phys. Chem. C. **121**, 1162–1170 (2017)
21. Rao, R.G., Blume, R., Hansen, T.W., Fuentes, E., Dreyer, K., Moldovan, S., Ersen, O., Hibbitts, D.D., Chabal, Y.J., Schlögl, R., Tessonnier, J.P.: Interfacial charge distributions in carbon-supported palladium catalysts. Nat. Commun. **8**, 340 (2017)
22. Sa-nguanprang, S., Phuruangrat, A., Karthik, K., Thongtem, S., Thongtem, T.: Tartaric acid-assisted precipitation of visible light-driven Ce-doped ZnO nanoparticles used for photodegradation of methylene blue. J. Aust. Ceram. Soc. **56**, 1029–1041 (2020)
23. Mou, H., Song, C., Zhou, Y., Zhang, B., Wang, D.: Design and synthesis of porous Ag/ZnO nanosheets assemblies as super photocatalysts for enhanced visible-light degradation of 4-nitrophenol and hydrogen evolution. Appl. Catal. B. **221**, 565–573 (2018)
24. Ainuddin, A.R., Yup, M.Z., Kamdi, Z., Hussin, R., Ibrahim, S.A.: Effects of Ag dopant and ultraviolet irradiation on structural properties of zinc oxide nanostructures. AIP Conf. Proc. **2045**, 020071 (2018)
25. Liang, H., Liu, S., Zhang, H., Wang, X., Wang, J.: New insight into the selective photocatalytic oxidation of RhB through a strategy of modulating radical generation. RSC Adv. **8**, 13625–13634 (2018)
26. Ghobadi, A., Ulusoy, T.G., Garifullin, R., Guler, M.O., Okyay, A.K.: A heterojunction design of single layer hole tunneling ZnO passivation wrapping around TiO_2 nanowires for superior photocatalytic performance. Sci. Rep. **6**, 30587 (2016)
27. Chen, X., Wu, Z., Liu, D., Gao, Z.: Preparation of ZnO photocatalyst for the efficient and rapid photocatalytic degradation of azo dyes. Nanoscale Res. Lett. **12**, 143 (2017)
28. Georgekutty, R., Seery, M.K., Pillai, S.C.: A highly efficient Ag-ZnO photocatalyst: synthesis, properties, and mechanism. J. Phys. Chem. C **112**, 13563–13570 (2008)